Inertial Centrifugal-Based Pre-filter for Spacecraft Life Support Systems

Juan H. Agui[1] and Jason P. Burns[2]
NASA Glenn Research Center, Cleveland, OH 44135

and

Robert D. Green[3]
NASA Glenn Research Center, Cleveland, OH 44135

The intrusion of planetary dust inside space vehicles on future lunar missions may lead to performance compromises of the cabin air-filtration system. The evasive character of the fine planetary dust, in particular lunar dust, could enable the dust to make its way through the seals and barriers of the EVA hatches and become airborne in the cabin. This can result in performance and capacity overload of the high efficiency filter media and particle separation systems. Adequate pre-filtration can substantially reduce the load on the higher efficiency components leading to smaller dust loads during surge and nominal dust loading conditions, thereby protecting and extending the life of these components. A particle separation concept, based on centrifugal separation, is being investigated for its application as a pre-filter. The concept has previously been proposed for application in the aircraft engine industry, as means of capturing corrosive dust and salt deposits that may harm the engine. The technique has the advantages of being passive, integrable to HVAC and space vehicle architecture, and has the potential for a high degree of particle separation when proper fluid dynamic design is applied. Computational Fluid Dynamics (CFD) and particle tracing modeling were used to arrive at an initial design for rapid prototyping and testing. If feasible, the concept can be integrated to the Scroll Filter System which is being developed by NASA to address the filtration demands on long during spaceflight and surface missions. This paper will describe the modeling results of this concept.

Nomenclature

d_{50}	=	cyclone separator cut size
K	=	porous media permeability
N	=	number counts
p	=	penetration
Q	=	flow rate
r	=	particle radius
κ	=	turbulent kinetic energy
ρ	=	particle density
ω	=	turbulent dissipation rate

I. Introduction

NASA's Artemis mission which is aimed at returning humans to the moon drives the current development of lunar dust mitigation technologies, including cabin air filtration. Air filters are an essential component of spacecraft Environmental Control and Life Support Systems (ECLSS) and are designed to control the generic dust environment inside the cabin. For reference, the International Space Station (ISS) uses pleated HEPA filter elements with a flat

---

[1] Aerospace Engineer, Thermal Systems and Transport Branch, 21000 Brookpark Rd, Mail Stop 77-5.
[2] Intern, Thermal Systems and Transport Branch, 21000 Brookpark Rd, Mail Stop 77-5.
[3] Aerospace Engineer, Thermal Systems and Transport Branch, 21000 Brookpark Rd, Mail Stop 86-12.

single layer screen pre-filter known as the Bacterial Filter Elements (BFE), which have operated successfully for over two decades.[1] However, the BFE's and other common cabin filters are designed for relatively clean to moderately clean environments, and not envisioned for environments with high particle concentrations, particularly of large particles (10's of micron and larger), that may be found in lunar dust.

Lunar surface missions will be faced with the intrusion of planetary dust inside space vehicles. The evasive character of the fine planetary dust, in particular lunar dust, could enable the dust to make its way through the seals and barriers of the EVA hatches and become airborne in the cabin. Although lunar dust is known to have a fine powdery nature, it has a broad particle size distribution from micrometers to millimeters in diameter, where more than 90% of the particles are above 10µm.[2] With the potential for large amounts of lunar dust to enter the cabin, the high likelihood of performance and capacity overload of the filter media and/or particle separation systems is a major mission risk. Therefore, there is a vital need for effective cabin filtration systems for future missions. This drives the need for adequate pre-filters for planetary missions where the planetary dust will compliment, and more than likely overwhelm, the levels of indoor dust. Effective pre-filters can substantially reduce the load on the higher efficiency components, leading to smaller dust loads to the latter during surge and nominal dust loading conditions, thereby protecting and extending the life of these components.

NASA has reported on developments of long-duration mission filters that extend life through regenerability and automated maintenance. The Scroll Filter System (SFS) is a filtration concept that is under development that provides multi-stage filtration, including inertial and media staged filtration, with built-in regenerability and automation that addresses the demands of long human exploration missions.[3,4] It was originally designed to handle cumulative generic dust loads inside the spacecraft over a long mission. However, the design of the multi-stage system can be adapted to handle planetary dust. The present concept is an inertial particle separator technique adapted from a patent applied in the aircraft engine industry, as means of capturing corrosive dust and salt deposits that may harm the engine.[5] In the aircraft application, the separator has the effect of inducing centrifugal forces on flowing particles, capturing these particles through orifice openings on the side wall of a diffuser duct with minimal disturbances to the main core flow. This new concept could serve as an add-on stage to the SFS or other media spacecraft filter system. This paper will present design details and modeling results in the development of the current inertial centrifugal-based separation technique.

II.   Centrifugal-based filtration

The adaptation of inertial separation filters for indoor environmental control and spacecraft ECLSS is challenging due to the specific ducted architecture and the typically low speeds associated in these applications. Thin panel filters with relatively large cross-sections are the mainstay of Heating Ventilation and Air Conditioning (HVAC) systems that comprise indoor environmental control. By contrast, inertial filters and separators require high speed flows through small inlets that are not inherently compatible with spacecraft ducted architecture. Inertial filtration typically also requires more power because of the substantial pressure drops associated with these flows, and the high decibel noise operation due to the high speed flows which adds to the challenges of their integration to spacecraft cabins.

The most recognizable inertial filters are cyclone separators, where particles above a certain diameter, determined by the cyclone design, are driven by centrifugal forces to the stagnation point on the separator. These devices are typically found in industrial settings for bulk processes and large dust containment, such as for sawdust or sand blasting particles. They are quite effective in removing 50% of particles larger than their design cut size, known as d_{50}. Cut sizes are nominally in the 10 µm range and larger for most standard cyclone separators, and down to 5 µ for premium efficiency cyclone separators used for small scale operations.[5]

For the spacecraft application, a two-dimensional centrifugal-based separator with a slender geometry compatible with spacecraft cabin duct architecture, e.g. the ISS air revitalization system (ARS), is adapted in the present work. The underlying concept borrows from the design of the aircraft engine application described above. The geometric design of this inertial filter provides a level of inertial separation to entrap a range of particle sizes above 10 µm. The separator can serve as pre-filter in a multistage spacecraft filtration system. The particles can be collected in a separate chamber in the separator, which can then be cleaned and serviced by the crew or it can have enough capacity to last the full mission.

Figure 1 shows the different geometries of the centrifugal separator investigated. The flow domain is shaded in grey and the arrows indicate flow directions at the inlets and outlets of these geometries. Figures 1a and 1b are symmetric geometries, with the geometry in Fig. 1b being the inverted geometry of Fig. 1a. Operationally what differentiates them is the location of the perforations along the flow path, where the large particles may enter the collection chamber. In Fig.1a, the perforated holes are located in the second turn of the S-curved pathway, and in Fig.

2

1b, the perforations are found in the first part of the S-curve. The S-curve provides high turning angles, i.e. high flow curvature that causes particles to acquire large inertial forces, forcing them to the outboard perforated walls before they have a chance to follow the streamline flow curvature. Lastly, Fig. 1c shows an asymmetric separator shape. There is only one main flow path compared to the two symmetric flow path cases. The flow path consists of a main large radius curve and a secondary small radius curve. The perforations can be located throughout or in certain sectors of the outer wall curve (the case shown has the perforations in the middle portion of the curve).

(a)

(b)

(c)
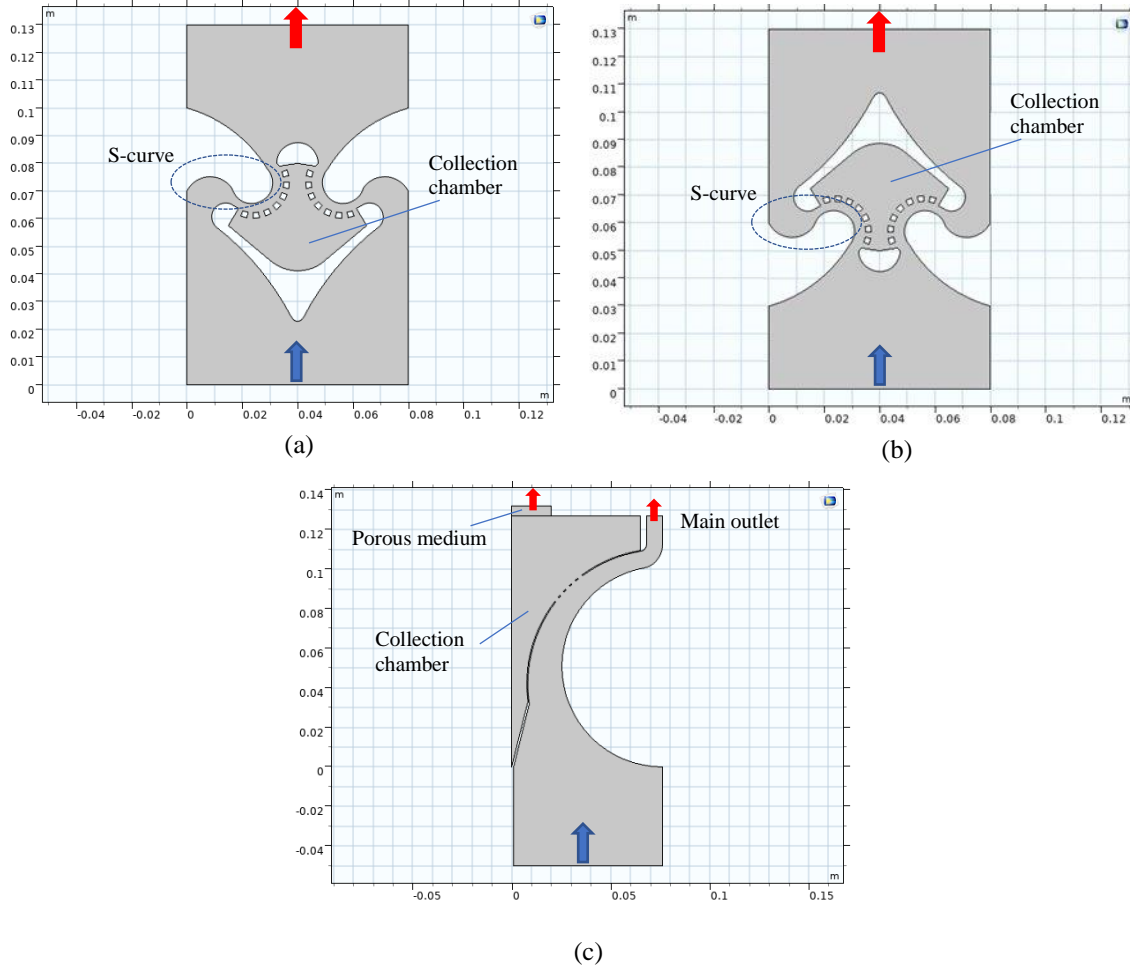
Figure 1: Geometrical designs for the centrifugal separator. (a) Symmetric geometry, (b) Inverted symmetric geometry, (c) Asymmetric geometry.

III. Modeling

The first phase in the development of the centrifugal separator involved modeling the flow and particle dynamics of the geometric designs. Modeling was performed using Computation Fluid Dynamics (CFD) and Lagrangian particle tracing solvers available in COMSOL Multiphysics software. A two-dimensional model of the centrifugal separator was generated using COMSOL's geometry module. Due to the high speed flows that are encountered, particularly in the narrow paths of the inertial filter where the Reynolds number can peak to high values, a turbulent flow model was chosen for the flow analysis. COMSOL's Shear Stress Transport (SST) model was used due to its high fidelity in resolving wall bounded flows.

Triangular meshes of the separator geometries were generated in COMSOL that were optimized for the turbulent flow solver. The meshes had approximately 20,000 and 60,000 elements for the symmetric and asymmetric geometries, with the meshes resolving the scales down to in the near wall regions. The turbulent Low Re wall condition was used to ensure zero velocity at the wall.

3

The particle tracing physics module in COMSOL solves for the trajectory of particle in a Lagrangian frame fixed to the moving particle. Particle drag is calculated through particle-fluid interactions coupled to the main flow solution. Stoke's drag using local flow conditions was applied to the particles. Gravity force was also applied to all the particle simulations.

Particle interactions with the separator walls could range from fully sticking to fully bouncing. Optionally, cases in which the particle sticks or bounces could be modeled to represent the degree of particle adhesion on the wall. In the present study the particle's kinetic energy was used to condition whether a particle would bounce or stick to the wall. The particle was allowed to bounce off the wall if the kinetic energy was above a threshold value. This value was set to a fraction of the maximum kinetic energy found inside the flow domain.

The flow domain for the asymmetric geometry included a porous medium domain at the top of the collection chamber, where the flow was modeled using Darcy's law and a laminar flow model. An outlet pressure constrained was set to a backpressure value of zero Pascal. Darcy's Law models the pressure drop as a function of inlet velocity which was coupled to the mean turbulent velocity in the adjacent main flow domain.

The modeling was performed in two steps. First, the steady-state flow solution was obtained for the main flow domain. Subsequently, the particle tracing model was run using an unsteady solver with the steady-state flow solution coupled to the particle's dynamics to provide the drag forces on the particle trajectories. Using the same flow solution, the particle tracing model was run several times by varying particle bounce condition at wall.

The modeling parameters are provided in Table 1. In these simulations, the inlet velocity was set to 0.5 m/s, which was based on a 1.7 m^3/min (60 cfm) flow rate going through a cross-section of the same width and length as the inlets of the present BFE's, i.e. a width and length of 65 cm and of 0.6 m respectively. The properties of the lunar regolith particles were also considered. The density of the particles was set to match the material density of the lunar regolith, representing approximately 3 g/cm^3.[5] The particle radius ranged from a radius of 2.5 to 39.5 µm which were uniformly distributed. Currently, there is no reliable data on the exact lunar dust particle size range and size distribution that is aerosolized in the spacecraft. Therefore, this analysis was focused on determining the collection efficiency as function particle size, independent of the number of particles of a specific size that enter the flow. Particles below 2.5 µm were assumed to pass through the inertial separator but then are caught subsequently by the media filters in the SFS or other finishing media filter. The number of particles released in the simulation was chosen to be large enough, 10000 particles, to provide sufficient resolution to determine capturing, or collection, efficiency. Earth gravity is applied in the current modeling since the results will be used to compare to ground based testing of separator designs, while future modeling will include the effects of reduced planetraty gravity and microgravity.

Table 1: Modeling parameters

| Parameters	variable	Value	units
Main flow domain			
Inlet flow speed	U_0	0.5	m/s
Outlet pressure	P_0	0	Pa
free stream turbulent kinetic energy	κ_0		
free-stream turbulent dissipation	ω_0		
Porous medium			
permeability	K	1.00E-12	m^{-2}
porosity	p	0.3	
Particle properties			
radius*	r	2.5 - 39.5	microns
density	ρ	3	g/cm^3
number of particles	N	10000	

*uniformly distributed

IV. Surface finish study

The ability of surfaces to capture particles entrained in the flow depends on several factors. The flowing particles have to first interact dynamically with the wall surface. Whether they stick or bounce depends first on the kinetic energy of the particles. If the wall is able to absorb some of the particle's kinetic energy causing the particles to pause or stall, its adhesion to the wall is determined by the surface physics of the particle and the wall. The finish, i.e. level

International Conference on Environmental Systems

of surface roughness, of the wall surface plays a big role in the level of adhesion. Gaier has studied the effects of lunar environments on the adhesion of lunar dust to various surfaces.[7]

A benchtop study was performed to assess the effect of surface finish on particle deposition on the wall surface from particles entrained in the flow. Coupons that were materially equivalent to the actual walls of the separators were prepared. Different coatings were tested to determine the most effective way to reduce particle buildup in unwanted areas. This test compared plain onyx (3D base material) with one to three layers of glossy paint (which provides a smooth and shiny reflective finish) for particle adhesion when a dynamic aerosol flow is directed alongside the surface. Microscopy and image editing software was used to accurately generate and compare data. The test setup consisted of a small flow channel where the coupons of the wall material could be inserted onto the sidewalls, and opposite to each other. An expanding jet flow emanating from a jar containing a small amount of JSC-1a lunar simulant and directed into the flow channel exposed the coupons to the lunar simulant particles.

Figure 2 shows a few of the representative coupon surfaces exposed to the particle flow. Figures 2a and 2b show coupons with one and two layers of glossy paint respectively that were exposed at the same time during one test (test 1), and separately Figs 2c and 2d show coupons with 2 and 3 layers of paint respectively that were exposed at the same time during a separate test (test 2). The images show the comparative build up and adhesion of dust with additional layers of paint. Based on the data collected, it appears that adding more layers of glossy paint reduces the probability of larger particles sticking to the surface. This results in a drop in overall particle buildup, and a lower particle number density on the tested surfaces. This would make the surface with three layers of glossy paint preferable for an inertial air filter to avoid any buildup in unwanted areas. Qualitatively each additional layer of paint appears to show a small drop in particle adhesion. From one to three coats there may be close to an overall 50% drop in the number of particles. This study form a basis for modeling the particle-wall interactions in our model.


(a)

(b)

(c)

(d)
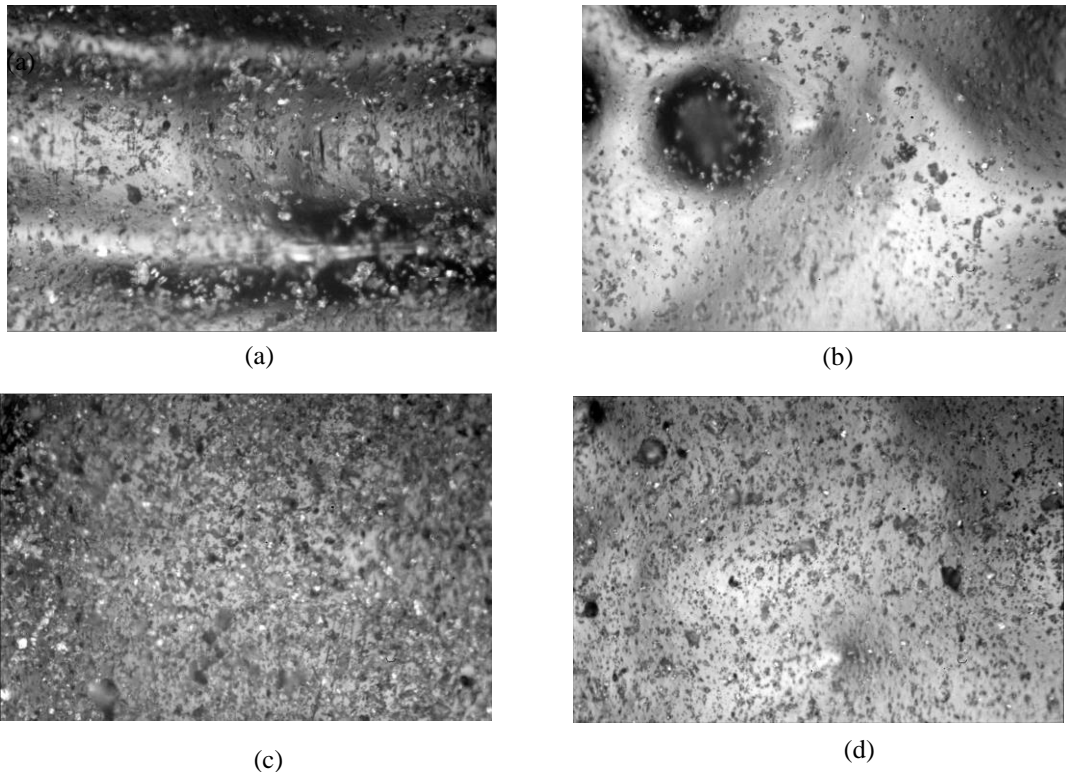
Figure 2: Microscopic images of the coupon surfaces with different layers of paint (a) one coat, test 1, (b) two coats, test 2, (c) two coats, test 2, (d) three coat, test 2.

V. Results

The flow fields generated by the various separator designs are shown in Fig.3. The plots show velocity magnitude contours and streamlines of the flow field. In the forward flow symmetric geometry, shown in Fig. 3a, the flow

5

converges as it approaches the S-curve region, on both side sides of the separator, and accelerates through the S-curve. High speed flow are reached in second leg of the S-curve, as indicated by the red velocity contour region there. Correspondingly, a high centripetal acceleration drives the flow around the bend of the S-curve, reaching values of 6000 to 7000 m/s^2. The particles traveling through this region of the curve will be subjected to a centrifugal acceleration of equivalent values, that would assist in propelling the particles through the wall perforations and into the collection chamber. In Fig 3b, the flow field in the inverted symmetric geometric design exhibits similar flow characteristics as in the forward geometry case. The highest flow speeds are found in the first part of the S-curve in this case, and reach slightly larger values than in the former case. A slightly larger centrifugal acceleration is also produced, up to 8000 m/s^2. The high centripetal accelerations found in both symmetric design leads to high centrifugal forces on the entrained particles, propelling them towards the outboard walls of the curves and subsequently driving them through the perforations and into the collection chamber. However, the flow that enters the collection chamber enters at low speeds, as indicated by the slightly lighter bluish shading in the collection region. The low speed flow entering the collection chamber diminishes the effect of entrapment of the particles. As will be shown, this was compensated for in the third asymmetric design.
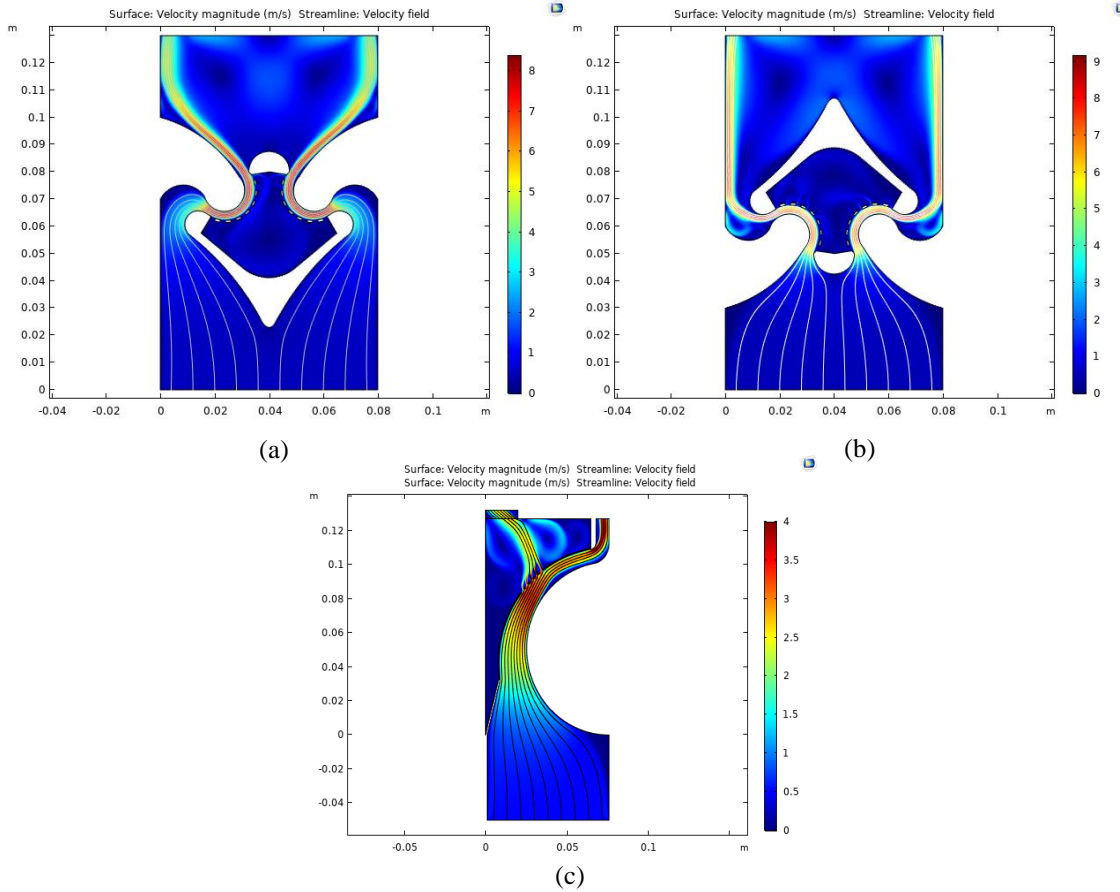

Figure 3: Velocity contour and streamline mappings of (a) Symmetric geometry, (b) Inverted symmetric , (c) Asymmetric geometry.

In the asymmetric design, shown in Fig. 3c, the flow is confined to one larger radius curved pathway where flow speeds reached 4 m/s, compared to the 8 to 9 m/s of the symmetric cases, for the same incoming flow rate. The smaller flow speeds induce smaller centrifugal accelerations on the particles. The centrifugal acceleration on particles was around 320 m/s^2, an order of magnitude lower than in the symmetric cases. However, the lower centrifugal acceleration is compensated with the longer arc path, provided by the large radius of curvature, in which the particles are given more time, by an order of magnitude, to reach the outboard wall of the curve while subjected to the centrifugal force. The d_{50} cut size can be selected and optimize with the location of the perforations along the curve into the collection chamber, and the spacing and diameter of the perforations (i.e. the open area ratio of the wall). Another compensation

6

International Conference on Environmental Systems

in this design is the use of a porous medium at the top of the collection chamber that generates a stream path and higher flow speeds from the perforations to the porous medium inlet as seen in Fig. 3c. This greatly increased the flow velocity through the perforations and facilitated the entrance of the particles into the chamber.

The pressure field inside the flow domains is shown in Fig 4. In the symmetric cases, the pressure builds up significantly ahead of the S-curve region. The pressures were found to increase by 30 Pa in the forward symmetric case, and up to 50 Pa in inverted symmetric case. Pressure drops across the whole separator were found to be about 35 Pa and 65 pa for the forward and inverted symmetric cases respectively. Compare to standard cyclone separators these pressure drops are quite small, and therefore the pressure drop benefit in these geometries is evident. One interesting finding was that the pressure drop in the forward symmetric case was about half that of the inverted symmetric case. In the collection chamber, a build up of pressure was found which produced a pressure gradient from the chamber to the S-curve region. In fact, this pressure gradient extended across the width of the flow path of the S-curve region, directed towards the inboard wall of the curved pathway. This countered to a degree the centrifugal force going in the opposite direction towards the outboard wall.


(a)

(b)

(c)
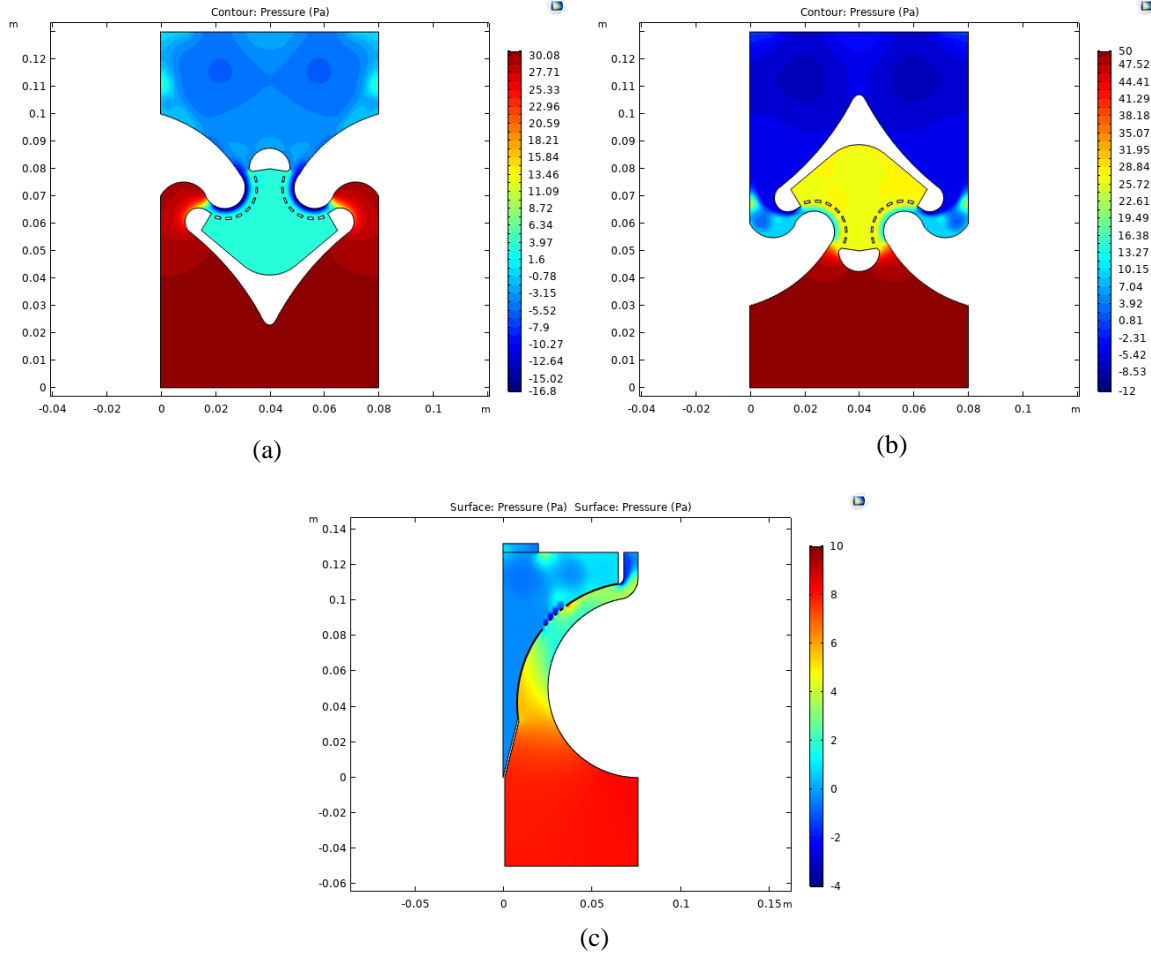
Figure 4: Pressure contours of (a) Symmetric geometry, (b) Inverted symmetric geometry, (c) Asymmetric geometry.

The pressure levels in the asymmetric case were quite lower than in the symmetric cases. The pressure drop across the separator in this case was found to be the lowest of three case, about 10 Pa. This is a significant improvement over standard cyclone separators. Unlike in the symmetric cases, there was no build of pressure in the collection chamber region. This result was mainly due to the presence of the porous medium which produced a pressure relief effect on the chamber. In addition, no discernable, or well-defined, pressure gradient was found across the curved pathway, to counter the centrifugal effect on particles projected towards the outboard wall of the curve.

7

Figure 5 shows a representative snapshot of the particle positions at the end of 3 seconds of simulation time. The particles are color coded by particle radius (in meters). All cases in this figure were simulated with reflecting walls, i.e. all particles bounced off the walls, to maximize particle transport to collection targets (outlet, collection chamber, or porous medium). These simulations are not representative of a lunar dust load because the particle size distribution (PSD) of the airborne lunar dust is not considered, and nor is particle adhesion to the walls. In fact, the PSD of the airborne lunar dust in the cabin is an unknown at this time. However, the final positions in these simulations are indicative of some of the inherent separation efficiencies and deficiencies in these geometries. In the symmetric case, only the smallest particles are caught in the collection chamber, and the largest particles end up leaving the separator. Similar results were found in the inverted symmetric geometry. This is actually the opposite of the desired effect of the separator. Although the collection of smallest particles is beneficial, the escape of the largest particles can excessively load the next filter stage, likely a media filter, which is designed to capture small particles. In the symmetric separator case, large particles tended to circulate around the corner regions, i.e. the initial bend of the S-curve path. The constrainment of large particles in this region could be problematic because it can cause an obstruction or blockage for subsequent particles. The asymmetric geometry, on the other hand, tended to capture most of the largest particles in the collection chamber. However, the particles at the outlet were not just of the smallest particles, but also of a range of different sizes. Again there is a concern that some large particles my leave the separator and cause problems at the next stage media filter, albeit not to the extent as in the symmetric geometries.

(a)

(b)

(c)
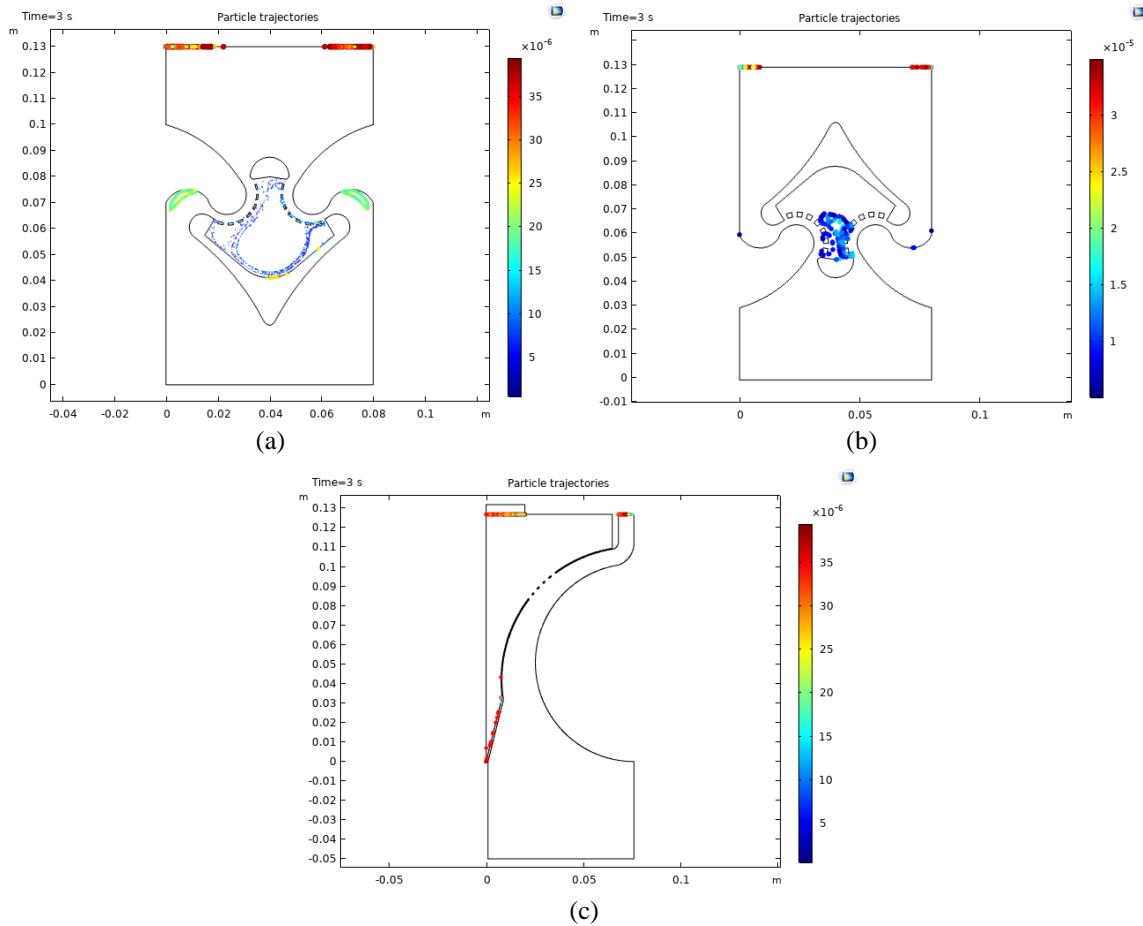
Figure 5: Particle trajectories of (a) Symmetric geometry, (b) Inverted symmetric geometry, (c) Asymmetric geometry.

When particles wall sticking was modeled it had a considerable effect on the particle trajectories. Simulations were performed by setting different levels of kinetic energy threshold for particles to bounce. When this energy was set to zero, all particles that reached the walls bounced off the walls. And when the kinetic energy was set a maximum value, all particles interacting with the walls stuck to the walls. Table 2 provides percentages of the general particle counts

8

on different parts of the geometry at the end of 3 seconds of simulation time. These values are not resolved for particle size. The values of particle counts at the outlet showed that the symmetric and inverted symmetric separators permitted the smallest number of particles to leave the separator. Although this appears advantageous, it was also found that a large percentage of particles, > 58%, tended to get stuck on the initial corner of the s-curve. This certainly will cause a quick blockage effect in this separator. This finding also provided insight that led to the design of the asymmetric separator which captures particles in the first bend of the curved pathway. If the particle counts in the collection chamber are used as the marker for separation efficiency, the asymmetric separator showed a clear advantage over the symmetric separator cases, capturing 25% to close to 60% of the particles for different particle wall bounce conditions. One case in the inverted symmetric geometry came close to the lower end of this collection efficiency range.

Table 2: Summary of particle trajectory analysis

Geometry	Wall condition (Energy required to bounce)	comment	particle diameter	outlet	corners	collection chamber	porous medium inlet	walls
	J		μ	(%)	(%)	(%)	(%)	(%)
symmetric	0.E+00		5 - 77	18.92	0	0.26		
symmetric	2.E-10		5 - 77	7.51	58.53	1		
symmetric	6.E-10	Max (all stick)	5 - 77	7.51	58.48	0.99		
symmetric inverted	2.E-10		5 - 77	10.29		31.62		
symmetric inverted	6.E-10	Max (all stick)	5 - 77	8.28		18.07		
asymmetric	0.E+00		5 - 77	32.09		59.78	59.51	0
asymmetric	1.E-11		5 - 77	26.44		58.69	36.2	13.58
asymmetric	3.E-11		5 - 77	23.45		45.64	23.76	17.33
asymmetric	5.E-11		5 - 77	18.7		40.48	19.67	24.93
asymmetric	8.E-11	Max (all stick)	5 - 77	13.61		25.75	14.79	43.77
asymmetric (no gravity)	0.E+00		5 - 77	29.35		55.58	55.46	1.41
asymmetric (no gravity)	8.E-11	Max (all stick)	5 - 77	13.34		26.05	14.09	44.38

Figure 6 shows a histogram of the particle counts at the asymmetric and symmetric separator outlets resolved by particle size. A comparison between particles sticking the wall and bouncing off the wall is also presented. The wall sticking interaction had the effect of cutting down the number of large particles that reached the outlet. This can be seen most clearly in both cases, where the largest particles went down from 82 µm for both cases to 30 µm and 10 µm respectively for the asymmetric and symmetric case. The real effect of particle sticking may be a combination of both cases. A more in depth study, including experimental data, of wall interactions and overall collection efficiencies using more refined particle properties and size distribution would be required to advance this model.
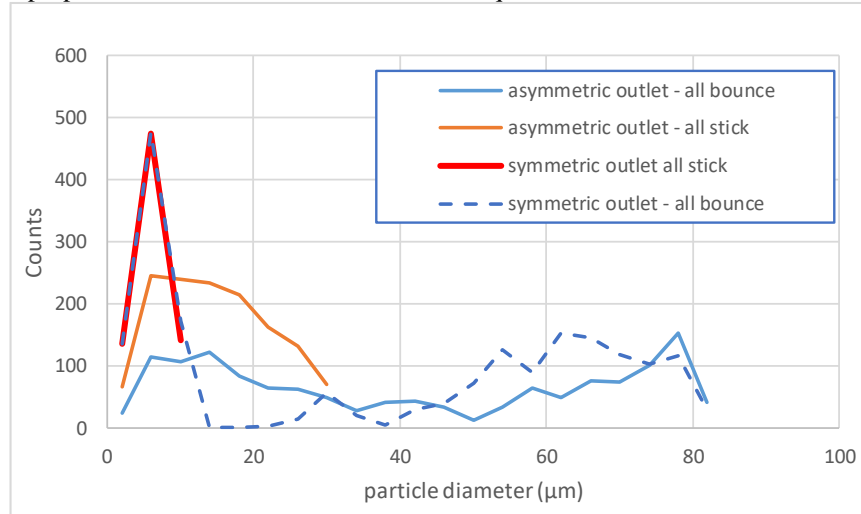
Figure 6: Particle size distribution of particles at the outlet boundary.

International Conference on Environmental Systems

VI. Conclusions and Future Work

A particle separation concept, based on centrifugal separation, is being investigated for its application as a pre-filter. Computational Fluid Dynamics (CFD) and particle tracking modeling was used to determine the performance of three different geometries and configurations. The modeling data provided a high degree of detail and performance characteristics on which to base a design for prototype and testing. Future work will involve 3D printed prototyping and testing in one of NASA's Glenn Research Center's (GRC's) filtration test stands.

References

[1]Green, R., Agui, J., Berger, G., Vijayakumar, R. and Perry, J., 2016, July. Filter efficiency and leak testing of returned ISS bacterial filter elements (BFEs) after 2.5 years of continuous operation. 46th International Conference on Environmental Systems.

[2]Carrier, W. D., III," Lunar Soil Grain Size Distribution," The Moon, Volume 6, Issue 3-4, pp. 250.

[3]Agui, J.H., 2019,"Scroll Filter System Development for Crewed Deep Space Missions, 49th International Conference on Environmental Systems, ICES-2019-2957-11 July 2019, Boston, Massachusetts

[4]Agui, J.H., Green, R.D. and Vijayakumar, R. "Development of a Multi-Stage Filter System for Cabin Ventilation Systems on the ISS and Future Deep Space Missions," 48th International Conference on Environmental SystemsICES-2018-1648-12July 2018, Albuquerque, New Mexico.

[5]Strangman, T.E., Morris, M.C., Baker, W.C., and Kington, H.L. (To Honeywell International Inc.), "Diffuser Particle Separator," U.S. Patent 7,581,397 (Sept. 1, 2009).

[6]Mackey, J., Agui, J., Crosby, K., Frye, B. and Sietz, T., 2010. Reduced Pressure Cyclone Separation Studies using Synthetic Lunar Regolith. In 40th International Conference on Environmental Systems.

[7]Gaier, J. and Sechkar, E., 2007, June. Lunar simulation in the lunar dust adhesion bell jar. In 45th AIAA Aerospace Sciences Meeting and Exhibit (p. 963).